PRELIMINARY, no distribution - vs. 3.2 (1/5/01): Collective flow of charged particles in Au+Au collisions for $\eta < |5.3|$ at $\sqrt{s_{_{NN}}} = 130$ GeV

B.B.Back[1], M.D.Baker[2], D.S.Barton[2], R.R.Betts[1,6], R.Bindel[7], A.Budzanowski[3], W.Busza[4], A.Carroll[2], M.P.Decowski[4], E.Garcia[7], N.George[1], K.Gulbrandsen[4], S.Gushue[2], C.Halliwell[6], J.Hamblen[8] G.A.Heintzelman[2], C.Henderson[4], R.Hołyński[3], D.Hofman[6], B.Holzman[6], E.Johnson[8], J.Kane[4], J.Katzy[4,6], N. Khan[8], W.Kucewicz[3], P.Kulinich[4], W.T.Lin[5], S.Manly[8], D.McLeod[6], J.Michałowski[3], A.Mignerey[7], J.Mulmenstadt[4],R.Nouicer[6], A.Olszewski[2,3], R.Pak[2], I.C.Park[8], H.Pernegger[4], C.Reed[4], L.P.Remsberg[2], M.Reuter[6], C.Roland[4], G.Roland[4], L.Rosenberg[4], P.Sarin[4], P.Sawicki[3], W.Skulski[8], S.G.Steadman[4], G.S.F.Stephans[4], P.Steinberg[2], M.Stodulski[3], A.Sukhanov[2], J.-L.Tang[5], R.Teng[8], A.Trzupek[3], C.Vale[4], G.J.van Nieuwenhuizen[4], R.Verdier[4], B.Wadsworth[4], F.L.H.Wolfs[8], B.Wosiek[3], K.Woźniak[3], A.H.Wuosmaa[1], B.Wysłouch[4]

(PHOBOS collaboration)

[1] Physics Division, Argonne National Laboratory, Argonne, IL 60439-4843

[2] Chemistry Department, Brookhaven National Laboratory, Upton, NY 11973-5000

[3] Institute of Nuclear Physics, Kraków, Poland

[4] Laboratory for Nuclear Science, Massachusetts Institute of Technology, Cambridge, MA 02139-4307

[5] Department of Physics, National Central University, Chung-Li, Taiwan

[6] Department of Physics, University of Illinois at Chicago, Chicago, IL 60607-7059

[7] Department of Chemistry, University of Maryland, College Park, MD 20742

[8] Department of Physics and Astronomy, University of Rochester, Rochester, NY 14627

(January 5, 2001)

This paper describes the first measurement of collective flow for charged particles in Au-Au collisons at $\sqrt{s_{_{NN}}} = 130$ GeV using the Phobos detector at the Relativistic Heavy Ion Collider (RHIC). Flow is observed as an anisotropy in the azimuthal charged particle hit distribution in the Phobos multiplicity detector. The size of the elliptic flow anisotropy (v_2), averaged over momenta and particle species, is observed to be ~7% for peripheral collisions at mid-rapidity, falling off with centrality and decreasing angle with the beampipe. Evidence for a directed flow signal is seen *** see comments in paper ***. Results are presented as a function of centrality and pseudorapidity (η) in the region of angular acceptance -5.0< η <5.3.

PACS numbers: 25.75.-q

The study of collective flow in ultrarelativistic heavy ion collisions is important because it can provide information on the initial geometry and the conditions present in early stages of the collision (the nuclear equation of state) [1]- [4], the degree of thermalization attained during the evolution of the collision [5] [6], and the possibility of a phase transition, such as the creation of a quark-gluon plasma (QGP) [1]- [3], [7]. In addition, collective flow can effect other measurables of interest, such as two particle correlation functions and the slopes of transverse momentum distributions [1] [8] [9].

Collective flow has been observed in nuclear collisions over a wide range of collision energies and species [1] [10]. As the collision conditions have evolved with time, so have the analysis technology and terminology. At higher energies, the discussion centers around elliptical and radial flow [1] [10] . Such flow has been observed at the AGS [11] [12], SPS [13]- [15], and most recently, at RHIC [16].

The analysis presented here is based on data taken between June and September, 2000 during the first RHIC physics run. Results are presented as a function of centrality for Au-Au collisions at $\sqrt{s_{_{NN}}} = 130$ GeV over a wide angular range, -5.0< η <5.3, where $\eta = -\ln\tan(\theta/2)$ and θ is the polar angle from the beam axis. These results serve to confirm the earlier report on the basic characteristics of elliptic flow at mid-rapidity, extend that result to substantially higher η, and provide the first evidence of directed flow at these energies.

The PHOBOS detector employs silicon pad detectors to perform tracking, vertex detection and multiplicity measurements. Details of the setup and the layout of the silicon sensors can be found elsewhere [17] [18]. For the running period relevant for this analysis, most of the silicon detectors were installed, including one full arm (16 layers) of the silicon spectrometer (SPECN), the first 6 layers of the second arm of the silicon spectrometer (SPECP), the full four layers of the silicon vertex detector (VTX), the silicon octagonal multiplicity detector (OCT), and the annular silicon ring multiplicity detectors (RN, RP). In total, the installed silicon sensors had *** readout channels, of which less than **2% were nonfunctional. The detector setup also included two sets of 16 scintillator counters ("paddle counters") located at distances of -3.21 m (PN) and 3.21 m (PP) from the nominal interaction point along the beam (z) axis. These counters served as the primary event selection trigger.

Monte Carlo (MC) simulations of the detector performance were based on the HIJING and RQMD event generators [20] [21] and the GEANT 3.21 simulation package, folding in the signal response for scintillator counters and silicon sensors.

The readout trigger selected events based on the coincidence of two or more hits in both PP and PN counters. This trigger accepted ∼85% of the total inelastic cross section. The centrality determination for the accepted events was based on the mean signal in the paddle counters with is proportional to the number of particles hitting these counters. The normalized paddle mean (normalized to the maximum value for the data set) was used as a centrality measure. More detail on the event triggering and centrality determinatio ncan be found in a previous publication [reference phobos prl].

During this run, Phobos data were taken with three different magnetic field settings in the spectrometer: zero field, positive field (+) and reversed field (-). The field strength falls off rapidly away from the center of the spectrometer arms. Consequently, the field configuration has a negligible effect on the trigger and paddle mean distribution in the data, which was confirmed by comparing distributions from the different data subsets.

For this analysis, trigger selection yielded approximately 7.6×10^5 events with + field, 1.7×10^5 events with zero field and 4.4×10^5 events with - field. These numbers reflect the removal of roughly 20% of the total data due to detector-associated irregularities observed in data processing diagnostics for signals emanating from the OCT, RN or RP detectors. The selected data were divided into 7 bins of centrality using the paddle mean distribution, as shown in the upper curve of Fig. 1.

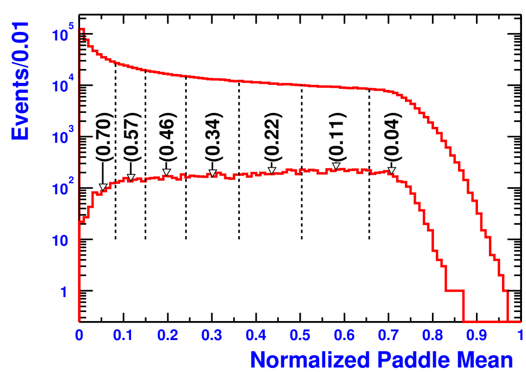

FIG. 1. The paddle mean signal distribution for triggered events (upper curve) and for data accepted for use in the final analysis (lower curve). The dashed lines delineate the centrality bins used in the analysis. The event-weighted mean position for each bin is shown along with the fraction of total events expected to have a larger normalized paddle mean.

The collision vertex was determined on an event-by-event basis by intersecting tracks reconstructed from hits in the first six planes of the two spectrometer arms (SPECN and SPECP). The magnetic field in this region of the detector is almost negligible, yielding straight line track segments and straightforward extrapolation. Specifically, all 3-hit combinations from 3 of the first 4 layers were determined and fit to a straight line. Track candidates were removed if the χ^2 probability of the fit was less than 10^{-8}. Hits on the missing one of the first four layers and layers 5 and 6 were associated with the nearest extrapolated 3-hit track candidate if the hit could be added to the track without reducing the χ^2 probability of the fit to less than 10^{-8}. The ambiguity of tracks sharing one or more common hits was settled by choosing the one with the higher fit χ^2 probability. The efficiency of this technique for central (highest occupancy) events was estimated from a study of simulated (Hijing) events to be ∼80%. In the same study the fake track level was determined to be ∼11% for central events, falling off for more peripheral events. These results were found to be independent of the state of the magnetic field.

The position of the primary collision vertex was determined on an event-by-event basis by fitting for the common vertex of the straight lines. Relative alignment of the spectrometer arms was accomplished with data by minimizing the vector difference between the independently reconstructed primary collision vertices. Therefore, the reconstructed vertex positions from SPECP and SPECN were generally consistent.

The vertex algorithm was applied for events with at least two tracks in SPECP and SPECN. The efficiency of finding a vertex was 34%, with the main loss due to collisions falling outside the spectrometer acceptance. The fitted vertex distributions in the transverse dimensions are shown in Fig. 2 for the zero field configuration. Those for the other field configurations are similar. In addition, vertices were required to fall within the fiducial region (-38cm< z_{vtx} <-30cm) due to the uniform and symmetric acceptance of the OCT subdetector in that region. 30772 events remained at this point in the analysis. In order to remove events with a pathological vertex reconstruction and reduce the potential for systematic effects, z_{vtx} was required to be consistent within 5 cm of the vertex position determined by an independent algorithm (leaving 20,028 events). The second algorithm determined z_{vtx} as the z position of the maximum in the azimuthally averaged hit density in the OCT subdetector. Finally, the reconstructed vertex position was required to be within 2σ of the average position (beam orbit) in each of the transverse dimensions.

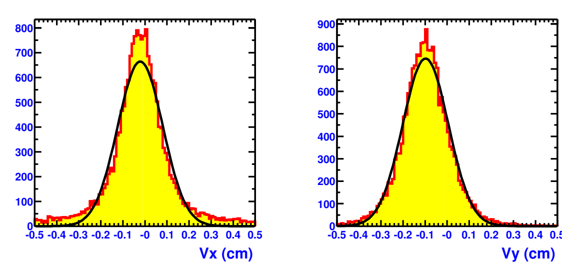

FIG. 2. Vertex distributions in x and y for the zero field data.

A total of 13169 events survived all cuts. The global acceptance for events used in the analysis was ∼1%. The paddle mean distribution for the accepted events is shown as the lower curve in Fig. 1. The vertex position resolution for events passing all cuts was estimated from simulated data to be ∼1 mm in x, ∼1 mm in y and ∼2 mm in z.

The flow analysis presented here is based on the charged particle hit anisotropy in the OCT, RP and RN subdetectors. The data for this analysis began as a stream of detector pixel energy depositions. These values were corrected for thickness variations in the silicon, normalized to 300 μm, and corrected for angle of incidence, assuming the charged particle to come from the reconstructed vertex position. At this point, pixels with energy depositions greater than 60 keV were taken to represent points of charged particle transit, known as hits.

Signals from hot or dead pixels were replaced with signals from corresponding mirror image pixels in η. This was done for less than 3% of pixels in the OCT and less than 1% of the pixels in RN and RP. Then an an $\eta-\phi$ pixel (bin) map of size 0.05×0.196 was imposed on the detector in software. The pixel map was binary. Software bins corresponding to regions of the detector containing at least one hit were assigned a value of 1. Otherwise they were assigned a value of 0. In order to smooth out the effect of the hardware pixelization, the hit location within the hardware pixel was smeared randomly with a flat distribution before it was transferred to the software bin map.

The flow analysis presented here follows the scheme proposed by Poskanzer and Voloshin [22]. The observed flow, v_n^{obs}, is given by the n^{th} harmonic Fourier coefficient of the $\eta-\phi$ map azimuthal hit distribution with respect to the event reaction plane, ψ_n.

$$\frac{dN}{d(\phi-\psi_n)} \sim 1+\sum_i 2v_n^{obs}cos[n(\phi-\psi_n)] \qquad (1)$$

ψ_n is the n_{th} harmonic event plane angle determined from the anisotropic flow itself as

$$\psi_n = tan^{-1}\left(\frac{\sum_i w_i sin(n\phi)}{\sum_i w_i cos(n\phi)}\right)/n, \qquad (2)$$

where the weights, w_i, are selected to optimize the reaction plane resolution and/or adjust for acceptance effects. The sums run over the occupied bins in the $\eta-\phi$ map. In order to avoid correlations, the evaluation of v_n and ψ_n and the event plane resolution must be done on independent sets of hits within the same event, so-called subevents.

In this analysis, several regions of eta acceptance were used as potential subevents. The particular choice of subevents depended on the calculation. The two regions at high-η corresponded to areas covered by the ring detectors, RN and RP, and encompassed -5.15< η <-2.76 and 3.35> η >5.34, respectively. In the mid-η range, covered by the OCT subdetector, one region (OCT-) extended from -2.0 to -0.1 in η while the other region (OCT+) encompassed η between 0.1 and 2.0. The gap between the two angular ranges in the OCT subdetector reduced short-range correlations between those subevents. For the determination of v_n in the positive (negative) η region of the detector, OCT- (OCT+) was used as the subevent to evaluate ψ_n. The eta regions presented for the final result were slightly smaller than the detector acceptance to avoid acceptance edge effects on the flow signal observed in Monte Carlo studies. The final results were found to be robust against the choice of subevent used in the evaluation of the event reaction plane so long as the chosen subevent contained sufficient statistics that the reaction plane resolution could be well determined.

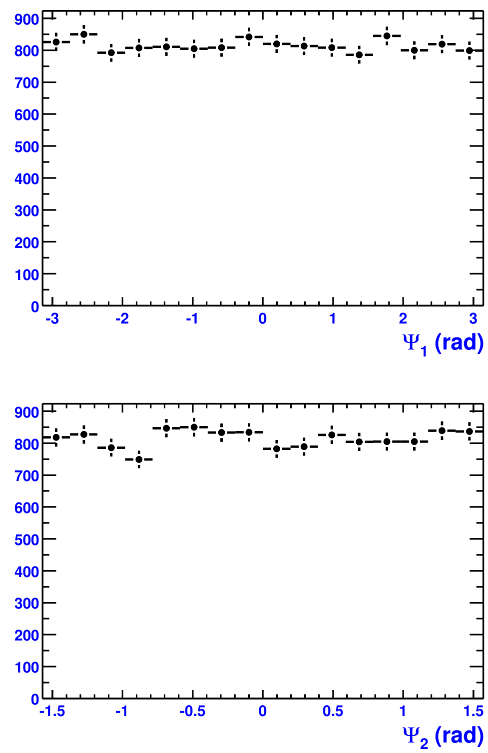

FIG. 3. The ψ_1 and ψ_2 distributions for this analysis after weighting.

The ψ_2 distribution is an excellent diagnostic for this analysis. ψ_2 is interpreted as the best estimate of the azimuthal angle of the event reaction plane, which is defined by the impact parameter and the beam axis. This distribution should be flat in the absence of detector effects. Structures in the raw ϕ hit and ψ_2 distributions were understood qualitatively from studies of simulated data as coming from gaps between sensors, channel-to-channel differences in ϕ phase space coverage, and the asymmetric production of background particles. All these effects were removed by setting w_i for the i^{th} $\eta-\phi$ map bin to be the inverse of the accumulated map bin sum for the i^{th} bin over the entire data set. With this weighting, the ψ_2 distribution was flat within statistics, fitting a flat line with χ^2/DOF=0.97. The flat line fit to the ψ_2 distribution before weighting had χ^2/DOF=55.3. The weighted

ψ_2 distribution is shown in Fig. 3.

In the scheme of Poskanzer and Voloshin [22], v_2^{obs} is evaluated by using the ϕ position of hits (or tracks) in one subevent (ϕ^b) with respect to the event plane reconstructed in the other subevent (ψ_2^a). In our analysis, this works in the limit of no detector pixelization. In conditions of high detector occupancy, our calculated v_2^{obs}, which we will call v_2^{pixel}, is less than the v_2^{obs} calculated in the limit of no pixelization. This was determined by extensive studies of simulated data samples with flow of various magnitudes injected into distributions of tracks with no flow as well as samples of Hijing events with flow injected prior to detector simulation. The fractional change in the observed v_2, v_2^{pixel}/v_2^{obs} was found to be independent of the amount of flow and could be described as C_o(1-Occ). In this parametrization, C_o is a constant that is approximately 1 in our analysis and Occ is the fractional eta-phi bin occupancy in the region of the eta-phi map where v_2 is being determined. The fractional change in v_2 due to this effect is shown in Fig 4. We explored the possibility of counting tracks in each bin by making use of the deposited energy information, but the lack of momentum information and the long tail of the Landau distribution prevented this technique from working. To summarize,in this analysis,

$$v_2^{obs} = \frac{v_2^{pixel}}{C_o(1-Occ)} = \frac{< cos[2(\phi^b - \psi_2^a)] >}{C_o(1-Occ)}. \qquad (3)$$

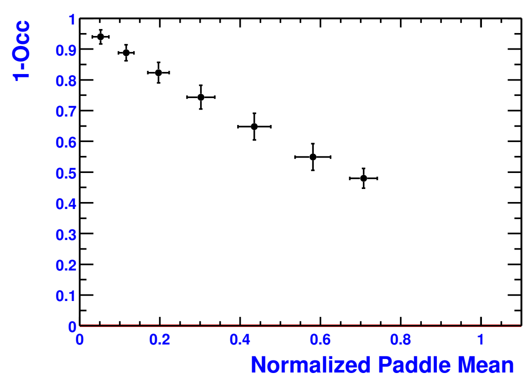

FIG. 4. C_o(1-Occ) for the data used in this analysis. This curve was used to correct v_2 for the effect of detector pixelization. *** this is similar to but not exactly the figure we will use ***

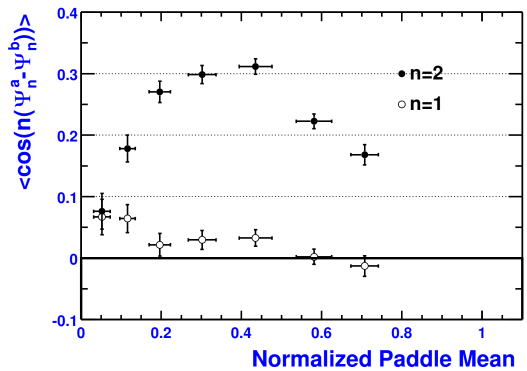

FIG. 5. Event plane angle correlations between subevents OCT- and OCT+ as a function of centrality bin.

The event plane resolution was determined from the correlation between the event planes in the subevents OCT+ and OCT- [22]. Fig. 5 shows this correlation for the first two harmonics for the full data set. It can be seen that this analysis is quite sensitive to elliptic flow, v_2, in our data. There is also some potential sensitivity to v_1 in the more peripheral events. The sensitivity of the analysis to v_2 can be seen graphically in Fig. 6 where the number of hits is plotted as a function of the azimuthal angle with respect to ψ_2 for different centralities. The number of hits plotted as a function of the azimuthal angle with respect to ψ_1 (for positive η) or $\psi_1 + \pi$ (for negative η) is shown in Fig. 7. The harmonic structure induced by directed flow is hinted at in the top curves corresponding to the more peripheral collisions.

The final value of the second harmonic flow coefficient, v_2, was derived by correcting v_2^{obs} with the measured event plane resolution. This amounted to dividing v_2^{obs} by the correlation between the reaction plane for one subevent, ψ_2^a and the reaction plane for the other subevent, ψ_2^b.

$$v_2 = \frac{v_2^{obs}}{\sqrt{< cos[2(\psi_2^a - \psi_2^b)] >}} \qquad (4)$$

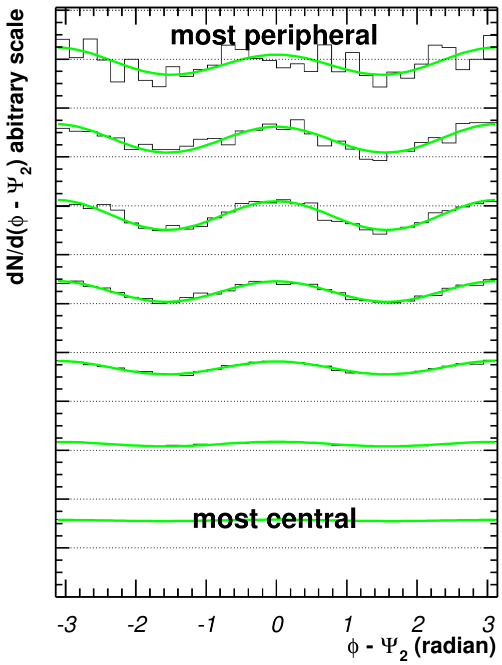

FIG. 6. dN/d(ϕ-ψ_2) as a function of centrality.

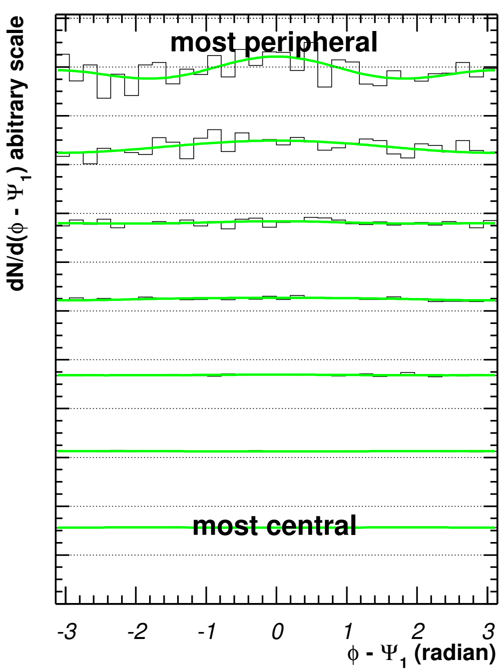

FIG. 7. dN/d(ϕ-ψ_1) as a function of centrality.

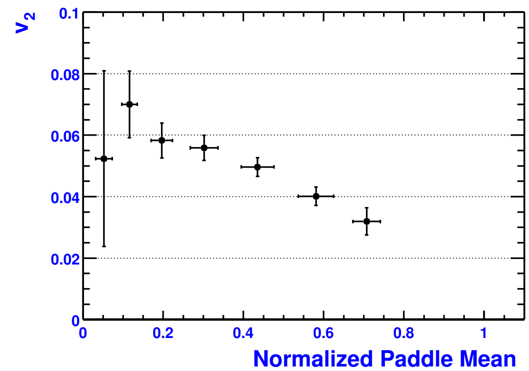

FIG. 8. Fully corrected measurement of elliptic flow, v_2, as a function of centrality. The error bars are statistical only.

The final value of v_2 is presented as a function of centrality in Fig. 8. Data falling within the region -1.0< η <1.0 contributed to this plot. The horizontal axis in Fig. 8 is in units of normalized paddle mean. The fraction of total events with a normalized paddle mean greater than that in each bin was estimated from simulated data and is shown in Fig. 1. This estimate has a 6% uncertainty arising from our lack of knowledge about our trigger efficiency for extremely peripheral events.

The η dependence of v_2, averaged over centrality, is shown in Fig. 9. For the sample of accepted events entering this plot, the average normalized paddle mean is 0.42.

********* V1 to be addressed before we release paper, but not before quark matter. We propose at QM to show v1 fourier plot and correlation plot and leave it at that. We do not have time to do the full study to understand the effect of pixelization on v1, which is needed before we can get a final numerical value ****

Numerous crosschecks of the analysis methodology were made. Events from a toy model with random track production were studied. No evidence for flow was seen. For simulated data where a specific amount of flow was imposed on the tracks at generator level and run through the detector simulation, the correct level of flow was extracted from the analysis, as was the case for toy model data with injected flow. Results from data with different field settings and different run periods are consistent. Finally, variation of the subevent used for the reaction plane definition in the analysis yielded consistent results.

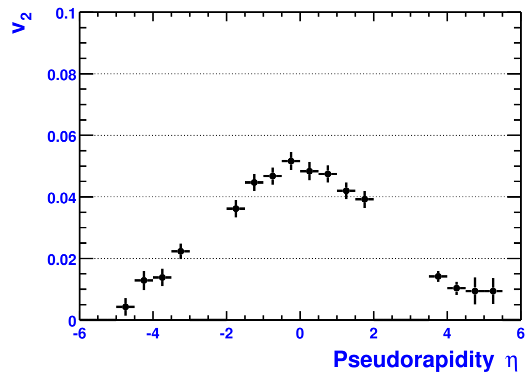

FIG. 9. Elliptic flow, averaged over centrality, as a function of η. The error bars are statistical only

Numerous sources of systematic error were investigated leading to an overall relative systematic error of 8% . The most significant error arose from the pixelization correction. The size of this error (6%, relative) was determined by examining the variation in the pixelization correction over a range of centrality and flow values in samples of simulated data. The systematic error arising from the hit definition (5% relative)was established by investigating the stability of the final result through a variation in the hit energy cut from 30-50 keV. A 3% relative systematic error was assigned to reflect our lack of knowledge of the beam orbit. This was determined by setting (x_{vtx},y_{vtx})=(0,0) for each event (rather than the reconstructed values) and observing the change in the final results. Several potential sources of systematic error were found to be negligible. These include variation of the vertexing algorithm changing the weighting matrix scheme (e.g., introducing a centrality dependence), and changing the method for dealing with hot and dead channels.

These results confirm the earlier mid-rapidity measurement by the STAR collaboration [16] and extend the measurement of flow out to $|\eta| < 5.3$. The extended angular coverage clearly shows a systematic dropoff in v_2 with $|\eta|$. The data indicate a weak directed flow signal in the most peripheral events. If this result holds up under futher scrutiny, this indicates that the flow at RHIC is in-plane and the sign of v_2 is positive.

*** we are thinking that we want to understand more about v1 before we send the paper out. In particular, we want to understand how the pixelization effects v1 ****

Acknowledgements: We acknowledge the generous support of the entire RHIC project personnel, C-A and Chemistry Departments at BNL. We thank Fermilab and CERN for help in silicon detector assembly. We thank the MIT School of Science and LNS for financial support. This work was partially supported by US DoE grants DE-AC02-98CH10886, DE-FG02-93ER40802, DE-FC02-94ER40818, DE-FG02-94ER40865, DE-FG02-99ER41099, W-31-109-ENG-38. NSF grants 9603486, 9722606 and 0072204. The Polish groups were partially supported by KBN grant 2 P03B 04916. The NCU group was partially supported by NSC of Taiwan under contract NSC 89-2112-M-008-024.

[1] W. Reisdorf and H.G. Ritter, Annu. Rev. Nucl. Part. Sci. **47** (1997) 663.
[2] H.Sorge, Phys. Rev. Lett. **82** (1999) 2048.
[3] P. Kolb, J. Sollfrank, and U. Heinz, Phys. Lett. **B459** (1999) 667.
[4] D. Teaney and E.V. Shuryak, Phys. Rev. Lett. **83** (1999)4951.
[5] P. Kolb, J. Sollfrank, and U. Heinz, hep-ph/0006129, 2000.
[6] S.A. Voloshin, A.M. Poskanzer, Phys. Lett. **B474** (2000) 27.
[7] For recent developments regarding QGP see Proceedings of the 14th Quark Matter conference, Nucl. Phys. **A661** (1999).
[8] see refs 20-23 in p and v prC 58 1998 1671
[9] H. Heiselberg and A. Levy, Phys. Rev. **C59** (1999) 2716.
[10] J.Y. Ollitrault, Phys. Rev. **D46** (1992) 229 and J.Y. Ollitrault, Nucl. Phys. **A638** (1998) 195.
[11] E877 Collaboration, J. Barrette *et al.*, Phys. Rev. **C55** (1997) 1420.
[12] E895 Collaboration, C. Pinkenburg *et al.*, Phys. Rev. Lett. **83** (1999) 1295.
[13] NA49 Collaboration, H. Appelshauser *et al.*, Phys. Rev. Lett. **80** (1998) 4136.
[14] WA93 Collaboration, M.M. Aggarwal *et al.*, Phys. Lett **B403** (1997) 390.
[15] WA98 Collaboration, M.M. Aggarwal *et al.*, Nucl. Phys. **A638** (1998) 459.
[16] STAR Collaboration, K.H. Ackermann *et al.*, ****.
[17] B.Back et al., Nucl. Phys. **A661** (1999) 690.
[18] H.Pernegger et al. Nucl. Instrum. Methods. **A419** (1998) 549.
[19] need reference for tof?
[20] M.Gyulassy and X.N.Wang, Phys. Rev. **D44** (1991) 3501. We used HIJING V1.35 (April 1998) with standard parameter settings.
[21] need reference for RQMD.
[22] A.M. Poskanzer and S.A. Voloshin, Phys. Rev. **C58** (1998) 1671.